Electronic Supplementary Material (ESI) for Journal of Materials Chemistry A.

Supporting information

B-site mixed cationic tetrahedral layer confined the concentration and mobility of interstitial oxygen in mellite family

Xiaohui Li,[a,b,c†] Xianyi Wei,[d,†] Xiaoge Wang,[b] Chenjie Lou,[e] Wenda Zhang,[d] Zhaoji Luo,[d] Jungu Xu,[d] Mingxue Tang,[e] Sihao Deng,[f] Lunhua He,[f,g] Xian-ran Xing,[c] Junliang Sun,[*b] and Xiaojun Kuang[*a,d]

[a] Guangxi Key Laboratory of Electrochemical and Magnetochemical Functional Materials, College of Chemistry and Bioengineering, Guilin University of Technology, Guilin 541004, People's Republic of China. E-mail address: kuangxj@glut.edu.cn.

[b] College of Chemistry and Molecular Engineering, Peking University, Beijing National Laboratory for Molecular Science (BNLMS), Beijing 100871, People's Republic of China. E-mail address: junliang.sun@pku.edu.cn

[c] Beijing Advanced Innovation Center for Materials Genome Engineering, Institute of Solid State Chemistry, University of Science and Technology Beijing, Beijing 100083, People's Republic of China.

[d] MOE Key Laboratory of New Processing Technology for Nonferrous Metal and Materials, Guangxi Key Laboratory of Optical and Electronic Materials and Devices, Guangxi Universities Key Laboratory of Nonferrous Metal Oxide Electronic Functional Materials and Devices, College of Materials Science and Engineering, Guilin University of Technology, Guilin 541004, People's Republic of China.

[e] Center for High Pressure Science and Technology Advanced Research, Beijing, 100193, People's Republic of China.

[f] Songshan Lake Materials Laboratory, Dongguan 523808, China; Spallation Neutron Source Science Center, Dongguan 523803, People's Republic of China.

[g] Beijing National Laboratory for Condensed Matter Physics, Institute of Physics, Chinese Academic of Sciences, Beijing 100190, People's Republic of China.

Table S1. Buckingham potential parameters for $Ca_2Ga_2GeO_7$.

Interaction	A (eV)	ρ (Å)	C (eV Å^6)	Y (e)	k (eV Å^{-2})
Ca^{2+}-O^{2-}	8573.82870	0.307992	560.4813	/	/
Ge^{4+}-O^{2-}	1479.96670	0.325647	16.80860	/	/
Ga^{3+}-O^{2-}	1625.72000	0.301900	5.790000	/	/
La^{3+}-O^{2-}	4579.23	0.30437	0.00	3	99999
O^{2-}-O^{2-}	22764.3000	0.149000	27.89000	-2.869	74.92

Table S2. Comparison of experimental and calculated lattice parameters in parent $Ca_2Ga_2GeO_7$.

Parameters	Calculated	Experimental	Δ(Calc.-Exp.)
$a = b$ (Å)	7.9715	7.8909	0.0806
c (Å)	5.0677	5.2060	-0.1383
$\alpha = \beta = \gamma$ (°)	90	90	0
Volume (Å^3)	322.0336	324.1583	-2.1247

Table S3. Comparison of experimental and calculated structure parameters in parent $Ca_2Ga_2GeO_7$.

Bond lengths	Calculate	Experimental	Δ(Calc.-Exp.)
Ca-O1 (×2) (Å)	2.5688	2.4706	0.0982
Ca-O2 (Å)	2.4812	2.4513	0.0299
Ca-O3 (Å)	2.5056	2.4668	0.0388
Ga1-O1(×4) (Å)	1.7861	1.8012	-0.0151
Ga2/Ge1-O1(×2) (Å)	1.7529	1.8131	-0.0602
Ga2/Ge1-O2 (Å)	1.7157	1.7475	-0.0318
Ga2/Ge1-O3 (Å)	1.7375	1.7835	-0.046

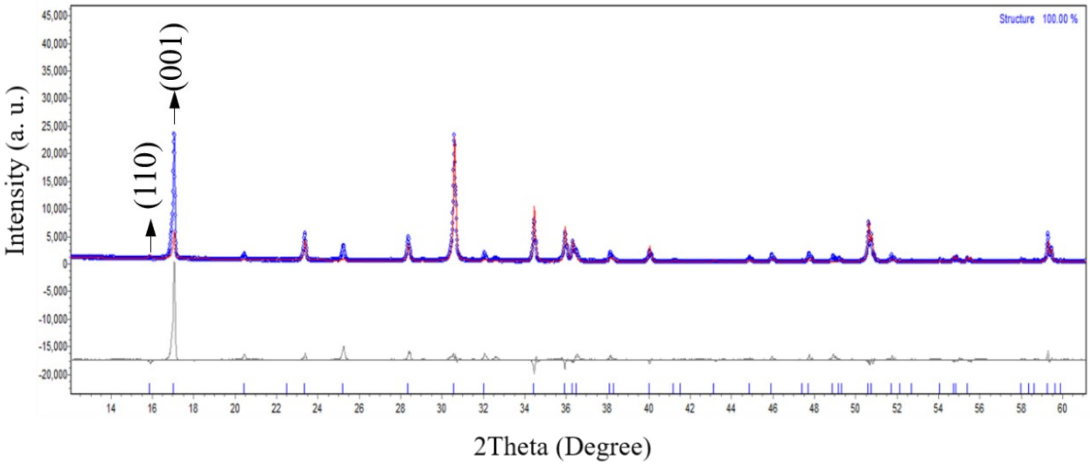

Figure S1. Rietveld refinement of XRD data for $Ca_{2-x}La_xGa_2GeO_{7+x/2}$ (x = 0.15).

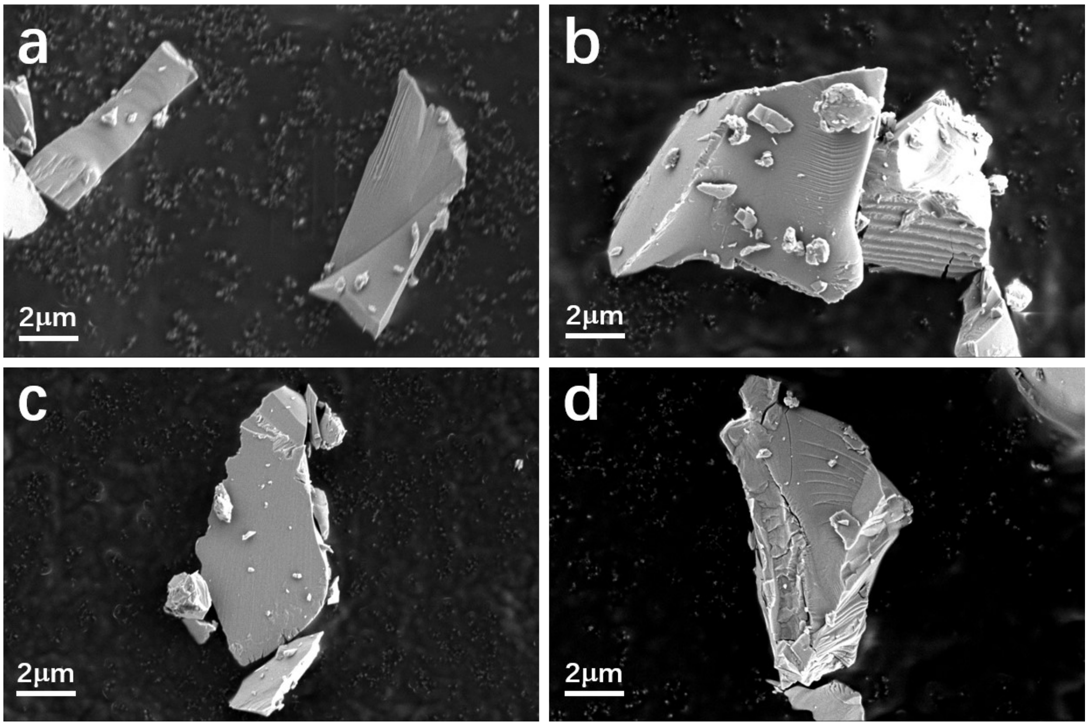

Figure S2. SEM images of $Ca_{2-x}La_xGa_2GeO_{7+x/2}$ samples: (a) x = 0, (b) x = 0.1 (c) x = 0.2 and (d) x = 0.3.

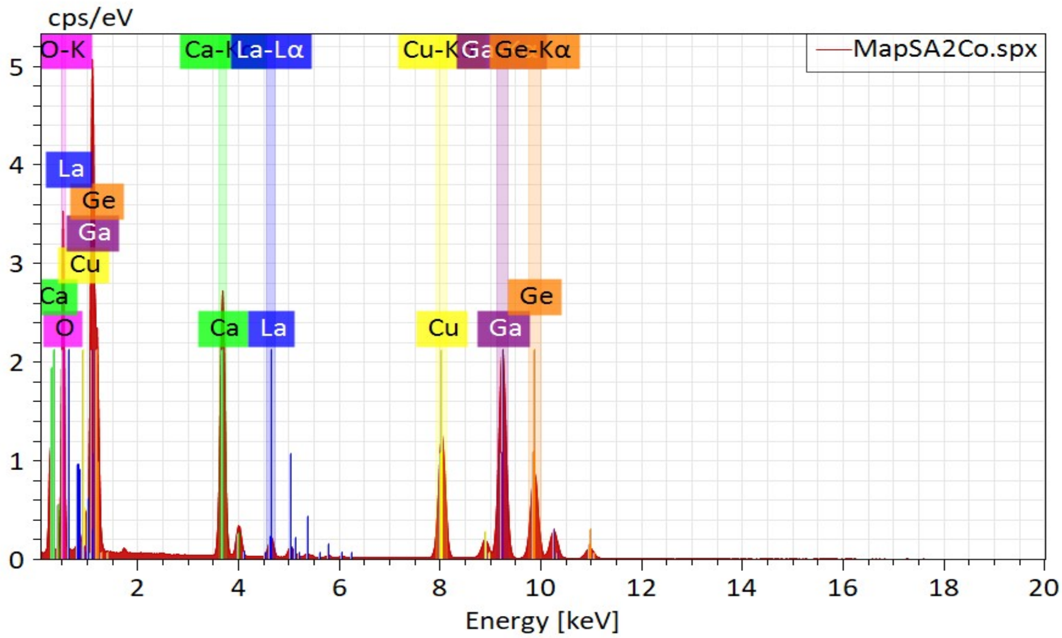

Figure S3. TEM-EDS data of $Ca_{2-x}La_xGa_2GeO_{7+x/2}$ (x = 0.15).

Table S4. The final refined structural parameters obtained from XRD data*.

Atom	Wyckoff site	x	y	z	occ	U_{iso} (Å^2)
Ca1	4e	0.1613(3)	0.6613(3)	0.4906(6)	0.925(9)	0.027(1)
La1	4e	0.1613(3)	0.6613(3)	0.4906(6)	0.072(9)	0.027(1)
Ga1	2a	0	0	0	1	0.015(1)
Ga2	4e	0.3561(2)	0.8561(2)	0.0368(4)	0.5	0.015(1)
Ge1	4e	0.3561(2)	0.8561(2)	0.0368(4)	0.5	0.029(2)
O1	8f	0.0905(2)	0.1621(3)	0.7985(5)	1	0.034 (1)
O2	4e	0.3576(2)	0.8576(2)	0.7011(5)	1	0.0205(8)
O3	2c	0	0.5	0.8097(9)	1	0.037(2)

*Space group: $P\bar{4}2_1m$, $a = b$ = 7.8926 (4)Å, c =5.2091 (3)Å, V = 324.493(4)Å^3.

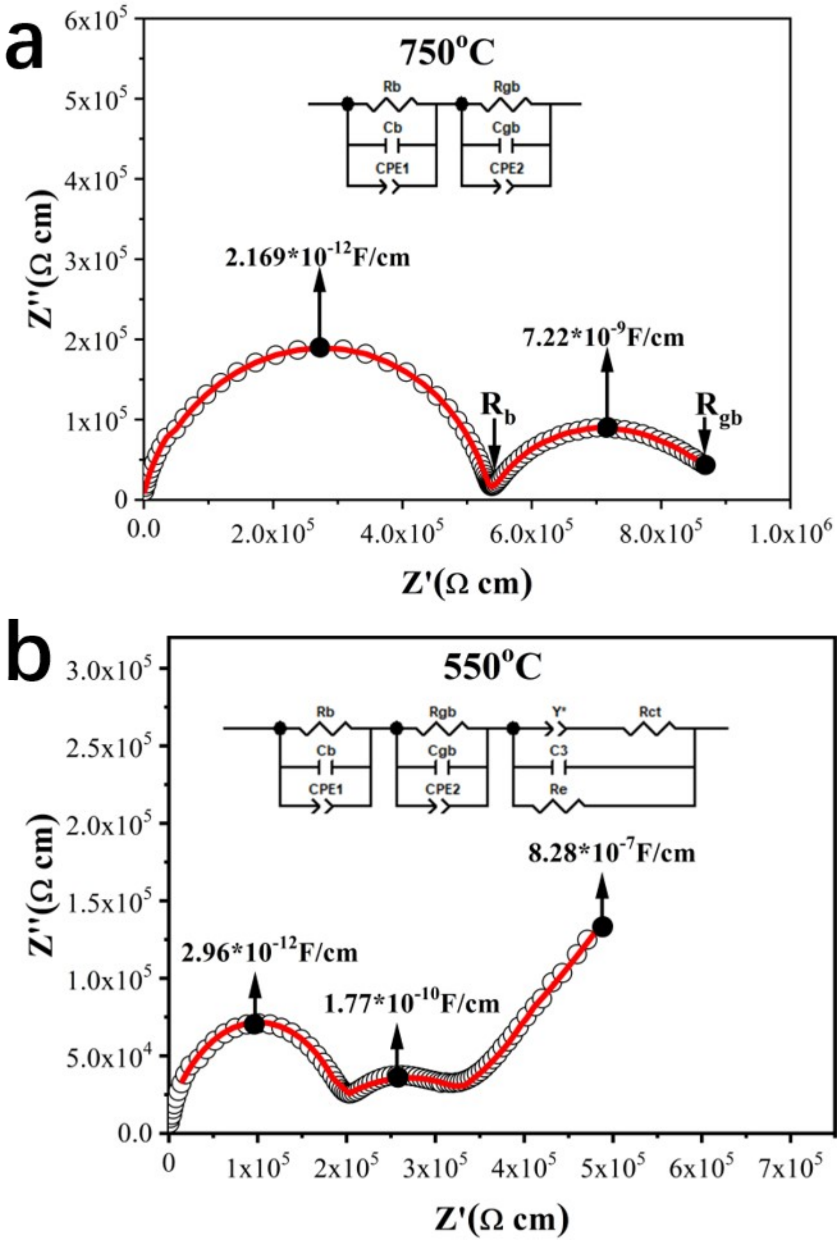

Figure S4. Typical complex impedance plots of (a) parent $Ca_2Ga_2GeO_7$ at 750 ºC and (b) $Ca_{1.85}La_{0.15}Ga_2GeO_{7.075}$ at 550 ºC.

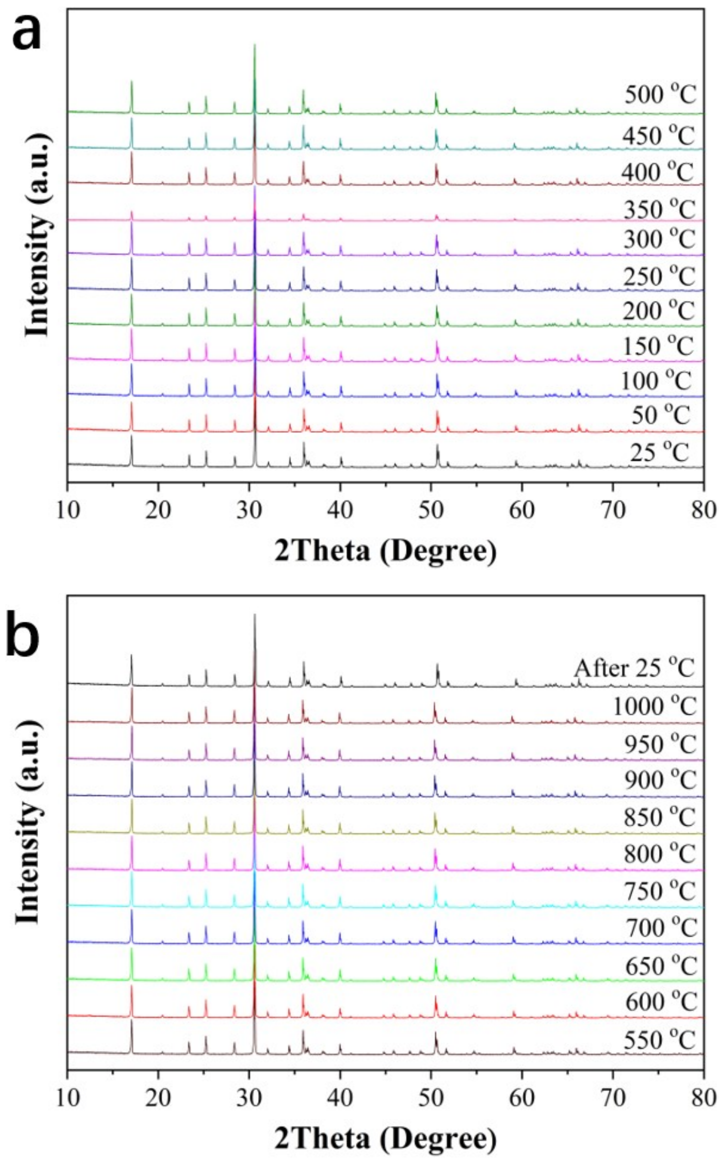

Figure S5. Variable temperature XRD patterns of parent $Ca_2Ga_2GeO_7$ in the temperature region of (a) 25-500 ºC and (b) 550-1000 ºC.

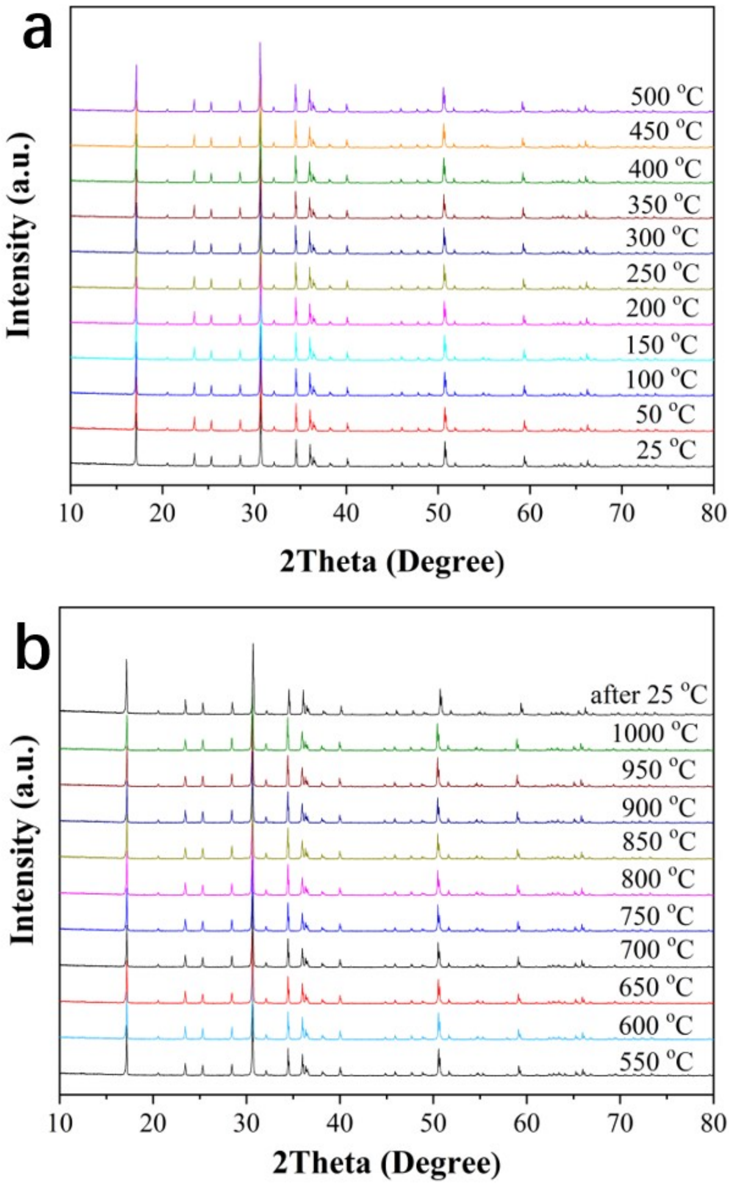

Figure S6. Variable temperature XRD patterns of $Ca_{1.85}La_{0.15}Ga_2GeO_{7.075}$ in the temperature region of (a) 25-500 ºC and (b) 550-1000 ºC.

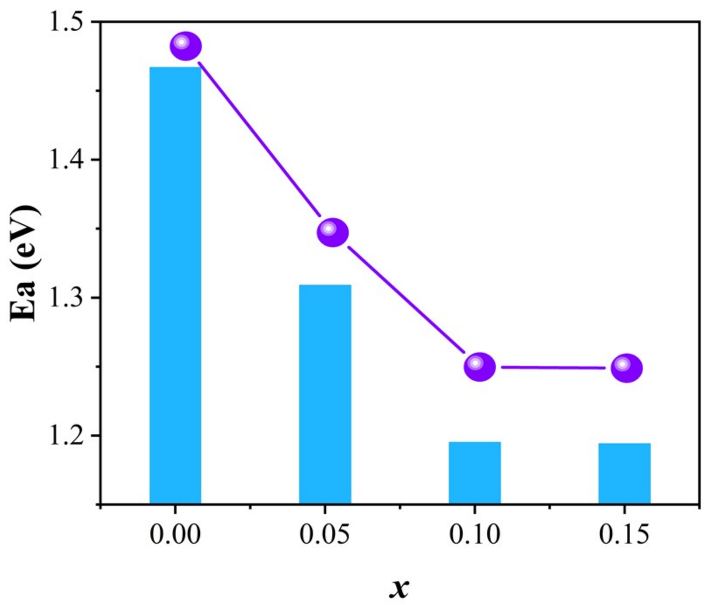

Figure S7. Activation energies of the $0 \leq x \leq 0.15$ compositions as a function of La^{3+} doping concentration.

Table S5. Anisotropic atomic displacement parameters of mellite $Ca_{1.85}La_{0.15}Ga_2GeO_{7.075}$ from NPD data.

Atom	Site	U_{11} (Å^2)	U_{22} (Å^2)	U_{33} (Å^2)	U_{12} (Å^2)	U_{13} (Å^2)	U_{23}(Å^2)
Ca1	4*e*	0.0286(15)	0.0286(15)	0.023(2)	-0.0164(19)	0.0004(15)	0.0004(15)
La1	4*e*	0.0286(15)	0.0286(15)	0.023(2)	-0.0164(19)	0.0004(15)	0.0004(15)
Ga1	2*a*	0.0081(11)	0.0081(11)	0.030(2);	0	0	0
Ga2	4*e*	0.0100(9)	0.0100(9)	0.066(5)	-0.010(5)	-0.008(4)	-0.008(4)
Ge1	4*e*	0.0100(9)	0.0100(9)	0.0101(19)	0.014(4)	0.009(2)	0.009(2)
O1	8*f*	0.0548(19)	0.0186(13)	0.0289(19)	-0.0163(11)	0.0151(13)	-0.0075(14)
O2	4*e*	0.0215(13)	0.0215(13)	0.0186(17)	-0.0134(19)	0.0151(13)	-0.0052(11)
O3	2*c*	0.0401(19)	0.0401(19)	0.031(4)	0.015(3)	0	0

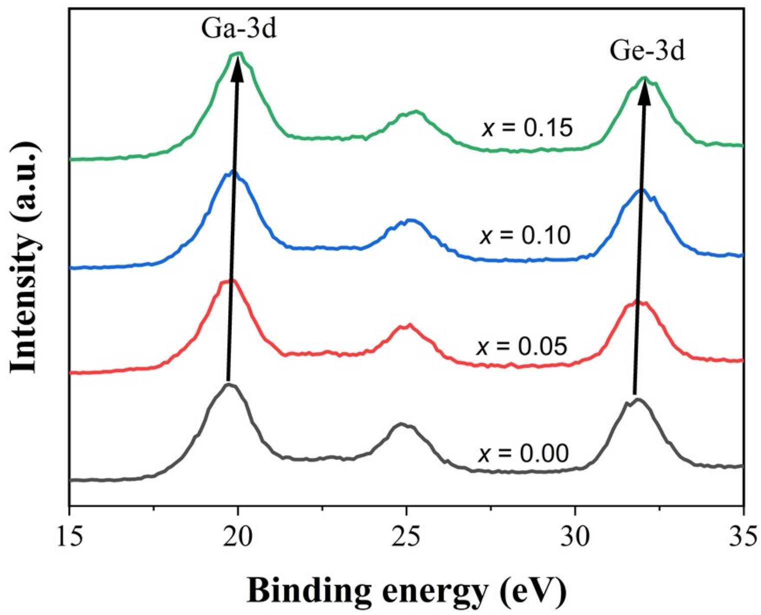

Figure S8. XPS spectra of Ga-3d and Ge-3d for $Ca_{2-x}La_xGa_2GeO_{7+x/2}$ ($0 \leq x \leq 0.15$).

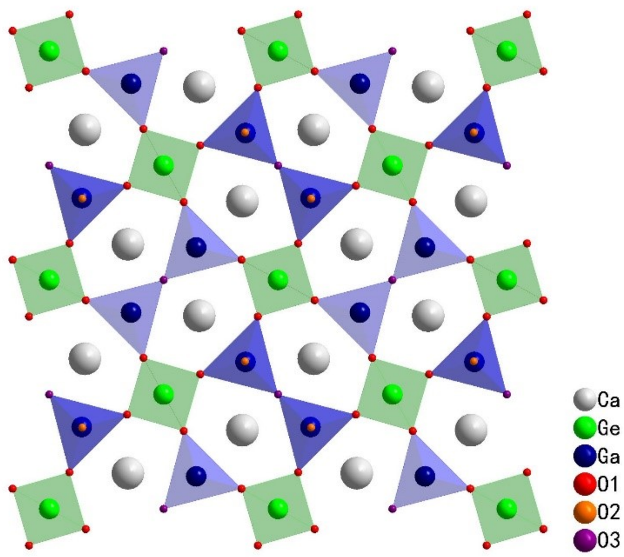

Figure S9. The Ga/Ge fully ordered structural model of $Ca_2Ga_2GeO_7$, where Ge occupies the 4-linked B' sites and Ga occupies the 3-linked B sites.

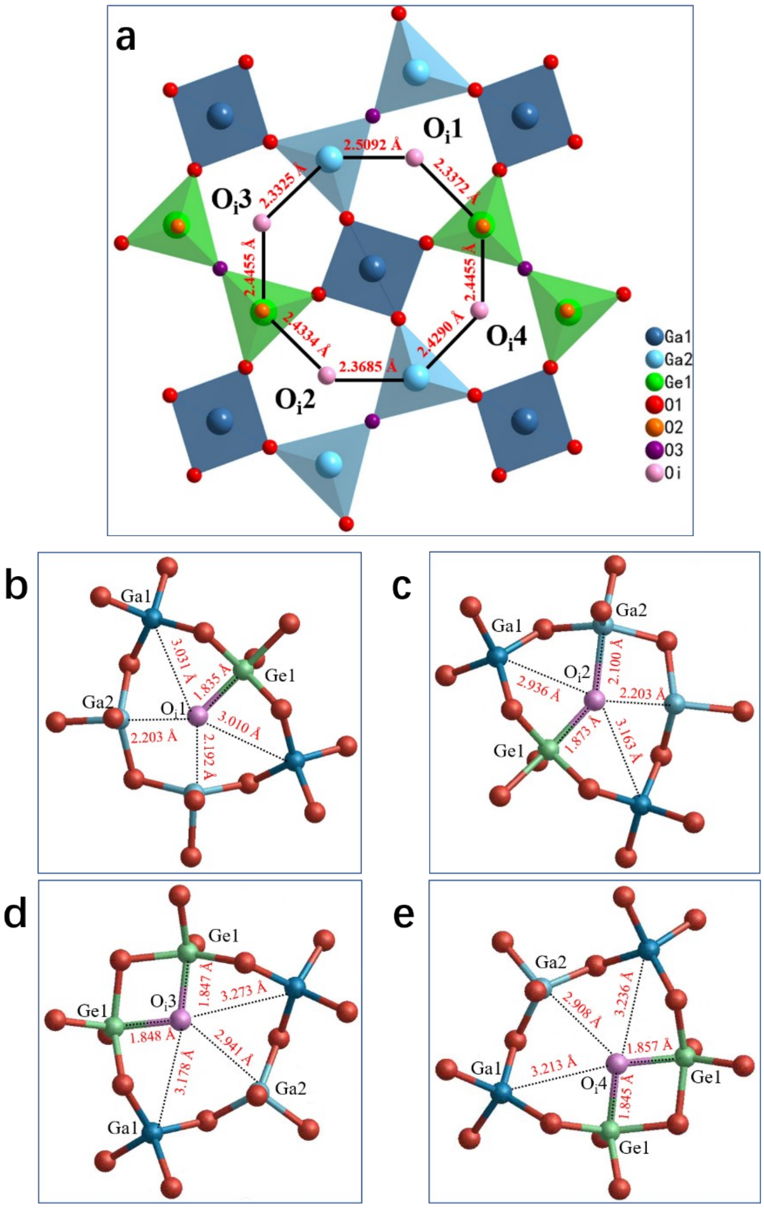

Figure S10. Structural models before (a) and after (b-e) structural optimization for the case of disordered occupation of Ga2 and Ge1.

Table S6. Defect formation energies of interstitial oxygen at different sites.

Oi	*x*	*y*	*z*	ΔE (eV)
O_i1	1.3189	5.3012	-0.0241	3.18
O_i2	6.7670	2.8680	0.0133	2.53
O_i3	4.8047	7.1763	5.2490	2.99
O_i4	3.2124	0.8375	5.2929	3.12

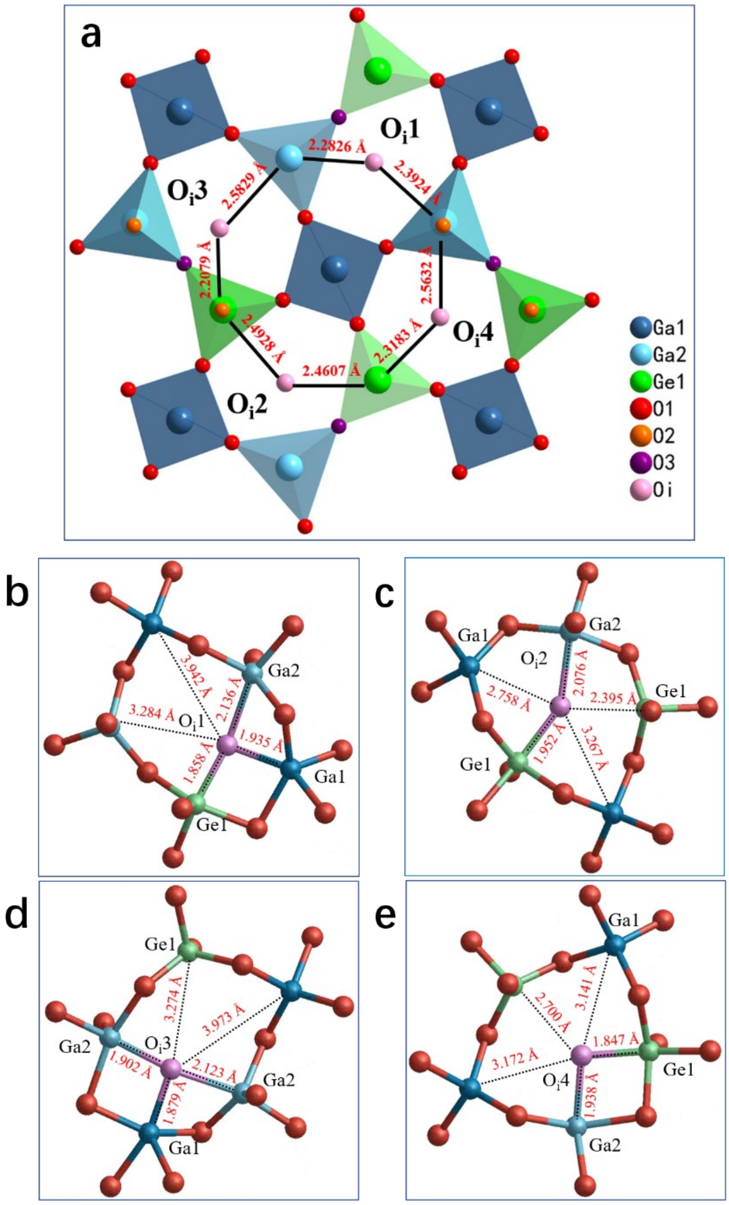

Figure S11. Structural models before (a) and after (b-e) structural optimization for the case of disordered occupation of Ga2 and Ge1.

Table S7. Defect formation energies of interstitial oxygen at different sites.

Oi	*x*	*y*	*z*	ΔE (eV)
O_i1	1.3189	5.3012	-0.0241	3.04
O_i2	6.7670	2.8680	0.0133	4.57
O_i3	4.8047	7.1763	5.2490	2.56
O_i4	3.2124	0.8375	5.2929	4.33

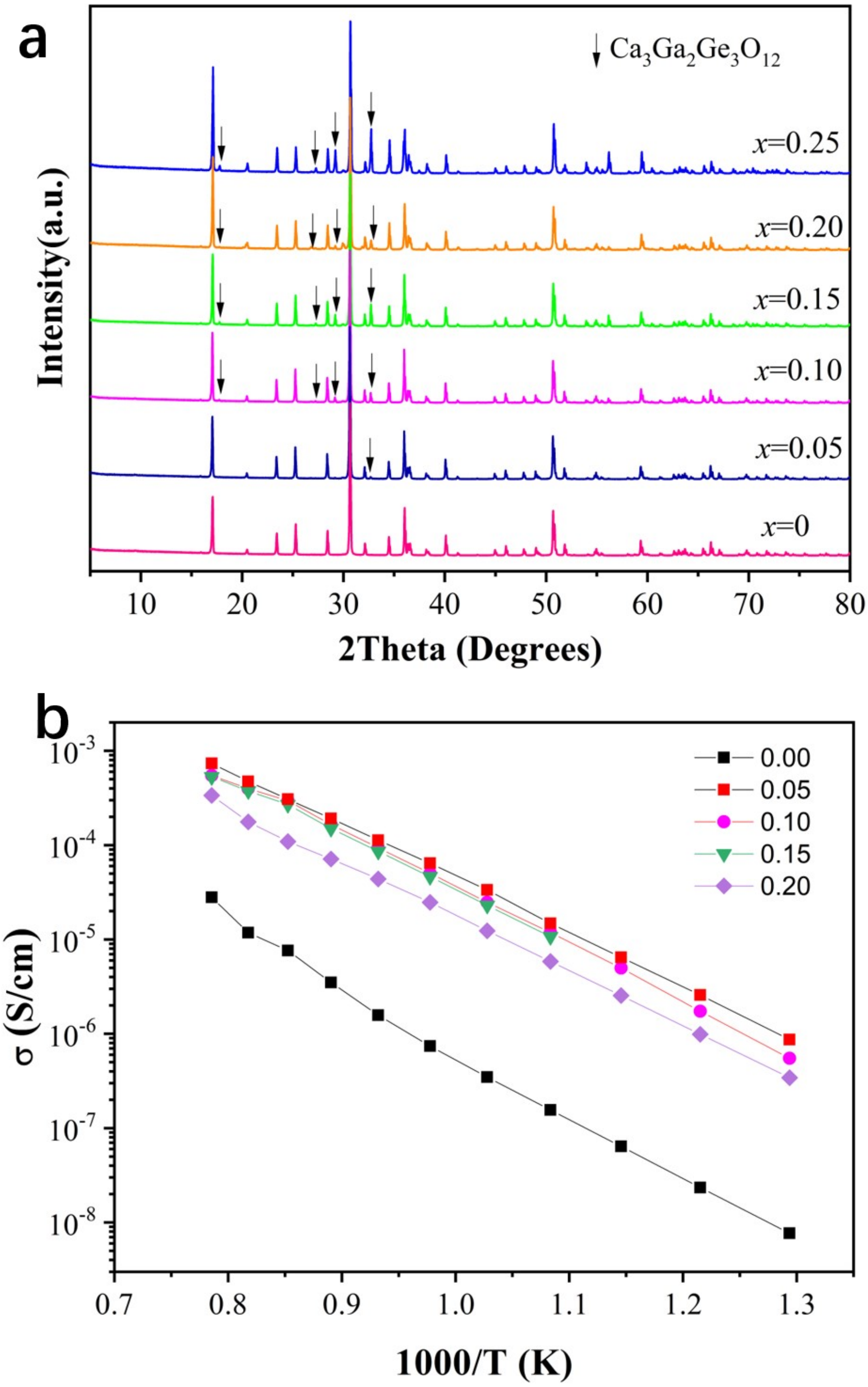

Figure S12. (a) XRD patterns and (b) conductivities of $Ca_2Ga_{2-x}Ge_{1+x}O_{7+x/2}$ ($0 \leq x \leq 0.20$). The black arrows denote the diffraction peak of impurity phase $Ca_3Ga_2Ge_3O_{12}$.

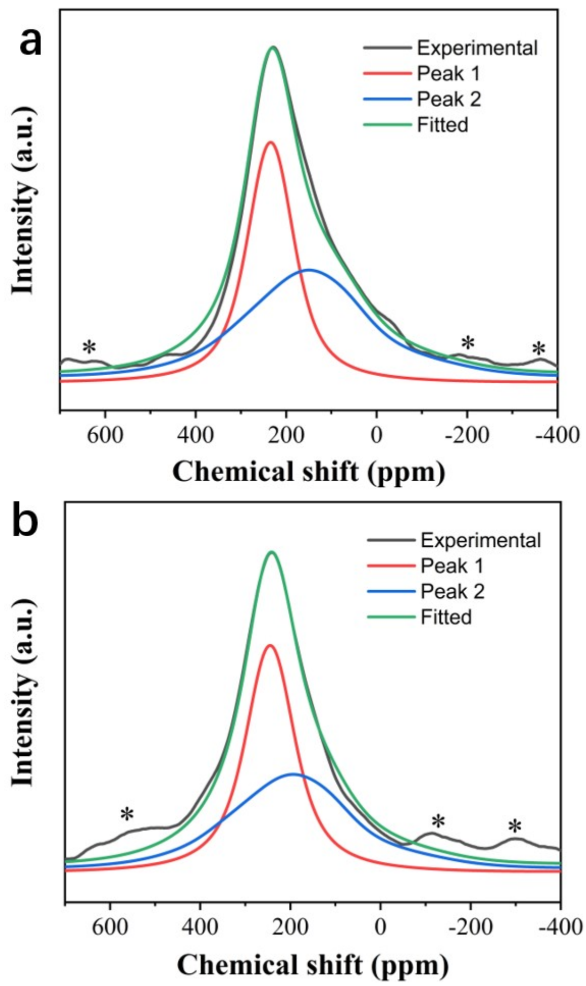

Figure S13. Experimental ^{71}Ga solid-state NMR spectra for (a) parent $Ca_2Ga_2GeO_7$ and (b) $Ca_{1.85}La_{0.15}Ga_2GeO_{7.075}$ at a magnetic field of 9.4T. The asterisks indicate spinning side bands.

Table S8. Simulated results from ^{71}Ga NMR data of parent $Ca_2Ga_2GeO_7$ and $Ca_{1.85}La_{0.15}Ga_2GeO_{7.075}$ at a magnetic field of 9.4 T.

Compositions	Site	Chemical shift (ppm)	C_Q (MHz)	η	Proportion (%)	Theoretical proportion (%)
$Ca_2Ga_2GeO_7$	Ga1	217	5.3	0.9	50%	50%
	Ga2	254	2.2	0.1	50%	50%
$Ca_{1.85}La_{0.15}Ga_2GeO_{7.075}$	Ga1	211	5.3	0.9	54%	50%
	Ga2	244	2.1	1.0	46%	50%

Experimental details of ^{71}Ga NMR measurement at lower magnetic field: Solid-state ^{71}Ga nuclear magnetic resonance (NMR) spectra at a magnetic field of 9.4 T were recorded on Bruker advance III 400 MHz WB spectrometer equipped with WVT 4 mm CP/MAS double resonance probe head operating at a ^{71}Ga Larmor frequency of 122.08 MHz. Spectra at 10 kHz MAS were recorded using a single pulse sequence of 2.0 μs (Nominal radio frequency field amplitude is 62.5 kHz, corresponding to a nominal flip angle of 45°), with 2048-3600 scans for each composition. All the spectra were collected at room temperature, and the chemical shifts were referenced to a standard aqueous solution of 1.0 M $Ga(NO_3)_3$ (0 ppm).

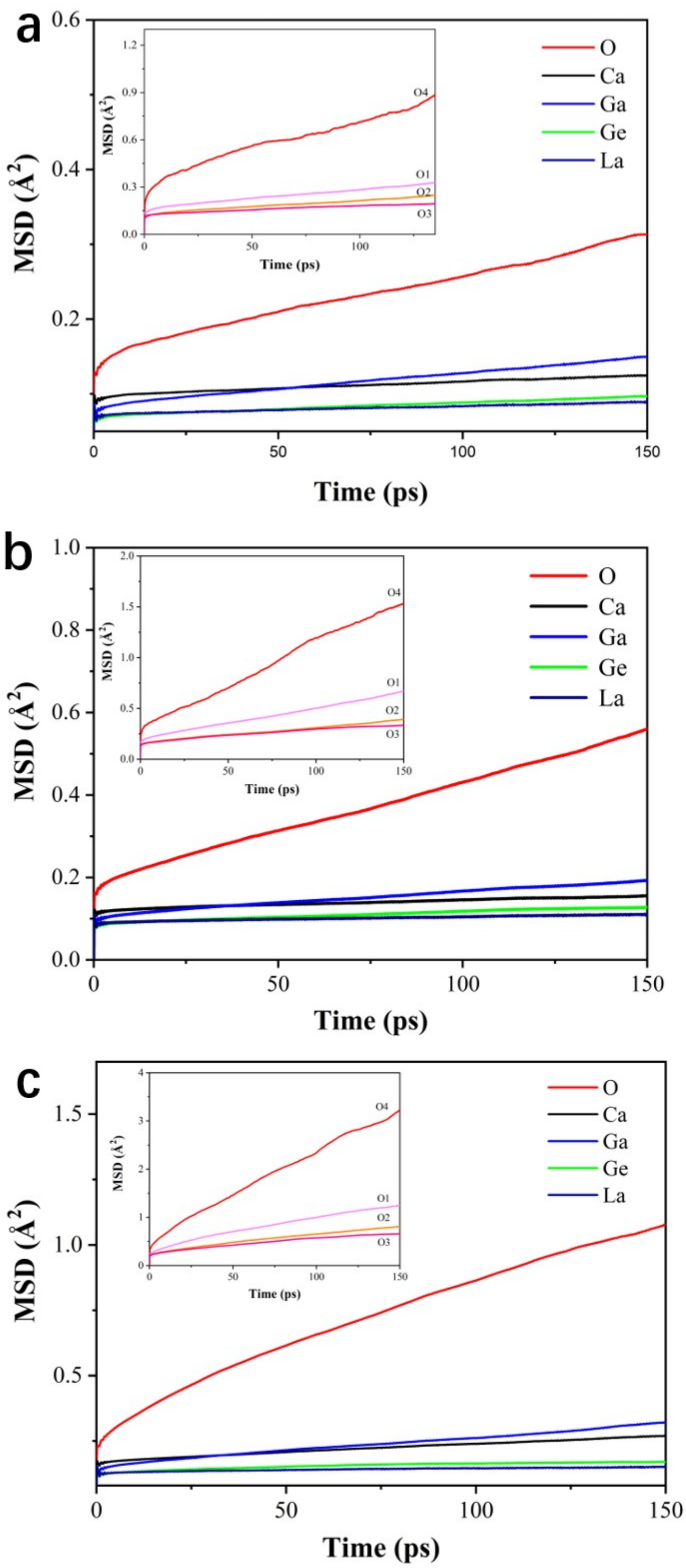

Figure S14. Mean square displacements of Ca, Ga, Ge, skeletal oxygen O1, O1, O3 and interstitial O4 as function of time at (a) 873 K, (b) 1073K and (c) 1273K.

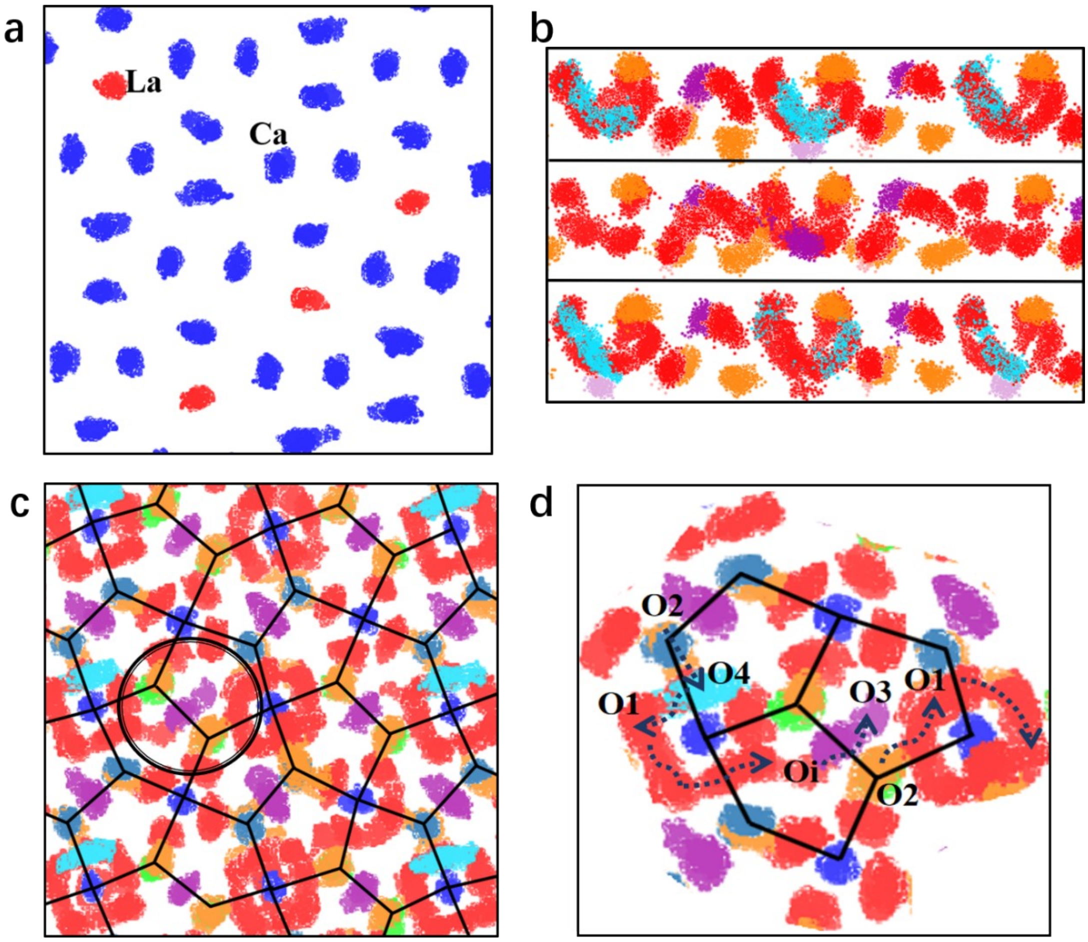

Figure S15. Scatter plots of (a) La^{3+} and Ca^{2+} positions along [001] direction, and oxide ion positions along (b) [010] and (c) [001] directions within 0-150 ps at 1273 K, where blue, light blue, green, red, orange, purple and blue-green represent Ga1, Ga2, Ge1, O1, O2, O3 and O4 atoms respectively. (d) The enlarged plot for the region marked by the black circle in figure c, where the black linear pentagon represents the five-fold ring formed by the cornering-sharing Ga/GeO_4 tetrahedra, allowing for clearer analysis of the oxygen migration path.

Figures S15a-c show that all cations do not exhibit any migration, and only the oxide ions have highly anisotropic migration within the corner-sharing (Ga/Ge)O_4 tetrahedral layers. The migration path in Figure S15d from O2 to O3 via O2-O1-Oi-O3, which involves the conversion of terminal oxygen O2 to bridging oxygen by the cooperative rotations and deformations of neighboring tetrahedra, demonstrating that the oxide ions are transported through the synergistic knock on motion of interstitial and framework oxygens.